The lowest place on Earth is subsiding—An InSAR (interferometric synthetic aperture radar) perspective

Gidon Baer*
Geological Survey of Israel, 30 Malkhe Yisrael Street, Jerusalem 95501, Israel

Uri Schattner
Geological Survey of Israel, 30 Malkhe Yisrael Street, Jerusalem 95501, Israel, and *Department of Geophysics and Planetary Sciences, Tel Aviv University, Ramat Aviv 69978, Israel*

Daniel Wachs
Geological Survey of Israel, 30 Malkhe Yisrael Street, Jerusalem 95501, Israel

David Sandwell
Cecil H. and Ida M. Green Institute of Geophysics and Planetary Physics, Scripps Institution of Oceanography, La Jolla, California 92093-0225, USA

Shimon Wdowinski
Department of Geophysics and Planetary Sciences, Tel Aviv University, Ramat Aviv 69978, Israel

Sam Frydman
Faculty of Civil Engineering, Technion–Israel Institute of Technology, Haifa 32000, Israel

ABSTRACT

Since the early 1990s, sinkholes and wide, shallow subsidence features (WSSFs) have become major problems along the Dead Sea shores in Israel and Jordan. Sinkholes are readily observed in the field, but their locations and timing are unpredictable. WSSFs are often difficult to observe in the field. However, once identified, they delineate zones of instability and increasing hazard. In this study we identify, characterize, and measure rates of subsidence along the Dead Sea shores by the interferometric synthetic aperture radar (InSAR) technique. We analyze 16 SAR scenes acquired during the years 1992 to 1999 by the European Remote Sensing ERS-1 and ERS-2 satellites. The interferograms span periods of between 2 and 71 months. WSSFs are observed in the Lisan Peninsula and along the Dead Sea shores, in a variety of appearances, including circular and elongate coastal depressions (a few hundred meters to a few kilometers in length), depressions in ancient alluvial fans, and depressions along salt-diapir margins. Phase differences measured in our interferograms correspond to subsidence rates generally in the range of 0–20 mm/yr within the studied period, with exceptional high rates that exceed 60 mm/yr in two specific regions. During the study period, the level of the Dead Sea and of the associated ground water has dropped by ~6 m. This water-level drop within an aquifer overlying fine-grained, marly layers, would be expected to have caused aquifer-system consolidation, resulting in gradual subsidence. Comparison of our InSAR observations with calculations of the expected consolidation shows that in areas where marl layers are known to compose part of the upper 30 m of the profile, estimated consolidation settlements are of the order of the measured subsidence. Our observations also show that in certain locations, subsidence appears to be structurally controlled by faults, seaward landslides, and salt domes. Gradual subsidence is unlikely to be directly related to the sinkholes, excluding the use of the WSSFs features as predictable precursors to sinkhole formation.

Keywords: consolidation, Dead Sea, ground-water level, land subsidence, synthetic aperture radar interferometry

INTRODUCTION

Land subsidence has become a global environmental and economic problem (Carbognin et al., 2000). In the United States, more than 80% of the identified subsidence features are associated with a drop in ground-water level or with oil or gas extraction (Galloway et al., 1999). Land subsidence may occur either as gradual settling or as sudden, sometimes catastrophic, collapse of the Earth's surface in sinkholes. In the 1990s, sinkholes became hazardous along the Dead Sea shores both in Israel and Jordan (Fig. 1; Arkin and Gilat, 2000; Swarieh et al., 2000; Wachs et al., 2000; Taqieddin et al., 2000). In places, they are surrounded by morphological depressions, a few tens of meters to a few kilometers wide, and a few centimeters to a few meters deep, caused by gradual land subsidence. Determining the spatial and, particularly, the temporal relationships between the sinkholes and the wide, shallow subsidence features (WSSFs) is important both for understanding the mechanism of the two, possibly related, phenomena and for possible prediction of sinkhole development.

During the twentieth century, the water level of the Dead Sea has dropped continuously from ~390 m below sea level (mbsl) in 1930

*E-mail: baer@mail.gsi.gov.il.
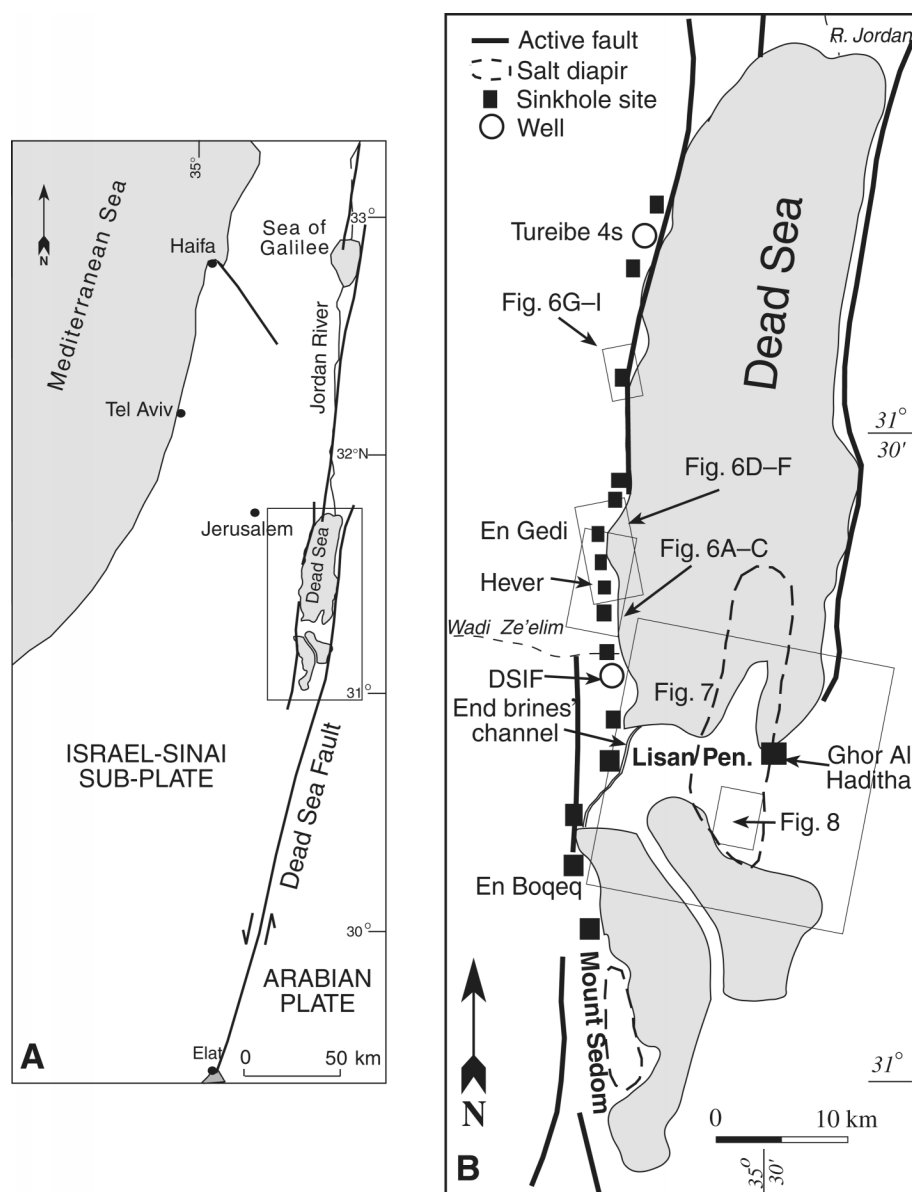
Figure 1. (A) General geographic and tectonic setting of the Dead Sea area (major faults after Bartov et al., 2000). (B) Location map of the Dead Sea showing the major active faults (after Bartov et al., 2000), major salt diapirs (after Neev and Hall, 1979), sinkhole sites (Wachs et al., 2000), water wells relevant to this study, and areas chosen for detailed analysis (Figs. 6, 7, 8).

and to measure rates of vertical displacement phenomena in the Dead Sea basin. We analyzed 16 SAR scenes spanning a period of 7 yr (1992–1999) to characterize the main occurrences of vertical movements. We then resolved the spatial and temporal relationships between InSAR-detected subsidence features and documented distribution of sinkholes (Itamar and Reizmann, 2000). Finally, we calculated the expected subsidence due to drop in ground-water level by numerical simulations, to better understand the mechanism by which WSSFs are formed.

GEOLOGIC BACKGROUND

The Dead Sea (Fig. 1) is the lowest place on the continental surface of the Earth, ~414 mbsl. It is located within one of the pull-apart basins that formed along the Dead Sea fault system (Fig. 1). The uplifted margins of the basin are built of Precambrian basement rocks overlain by Paleozoic to Cenozoic sedimentary and igneous rocks. Miocene to Holocene, mostly lacustrine and terrestrial sediments have accumulated within the basin (Picard, 1943; Zak, 1967). The upper few tens of meters along the Dead Sea shores consist of the late Pleistocene Lisan Formation (Begin et al., 1974) composed of alternations of crystalline aragonite and detrital material (mostly clay), overlain by the Holocene coarse and fine-grained detrital layers of the Ze'elim Formation (Yechieli, 1993). The relative abundance of fine-grained layers within the Ze'elim Formation increases eastward (Fig. 3). A salt layer, ~8–12 m thick and ~10,000 yr old, was encountered by several boreholes at depths greater than 20 m and was traced by seismic refraction studies along most of the western side of the Dead Sea (Wachs et al., 2000).

A thick (>2000 m) sequence of mostly marine salt with interbedded gypsum, shale, and dolomite rocks of Pliocene to Pleistocene age has built several salt diapirs in the Dead Sea area (Zak, 1967; Neev and Hall, 1979). In Mount Sedom (Fig. 1B), the diapir is exposed at the surface. Other diapirs (e.g., Lisan Peninsula) remain buried at varying depths (in places only ~100 m) below the surface (e.g., Bartov, 1999).

Sinkholes and WSSFs are found in two sedimentary environments along the Dead Sea shores: marginal alluvial fans and coastal mud flats (Wachs et al., 2000). At the surface there is a gradual transition between the two environments, whereas in the subsurface the layers interfinger (Fig. 3). Sinkholes are generally circular, 1–20 m wide, and may reach depths greater than 15 m. These features are generally

to 414 mbsl at the end of 1999 (Klein, 1985; Yechieli et al., 1995; Wachs et al., 2000). The average rate of water-level drop has increased since 1970, and since 1995, it has been ~1.2 m/yr. A corresponding drop in the level of the coastal ground water accompanies the Dead Sea water-level drop (Fig. 2). The combination of drop in ground-water level with fine-grained clastic layers may produce an unstable environment susceptible to landform deformation by compaction and regional subsi-

dence (Galloway et al., 1999; Wachs et al., 2000).

Recent developments in satellite geodesy techniques, and especially interferometric synthetic aperture radar (InSAR), introduced new tools to identify and measure very subtle vertical displacements (elevation change of ±10 mm) such as long-term subsidence features (Galloway et al., 1998; Amelung et al., 1999; Fielding et al., 1998). In this study, we have used InSAR to obtain spatially detailed maps
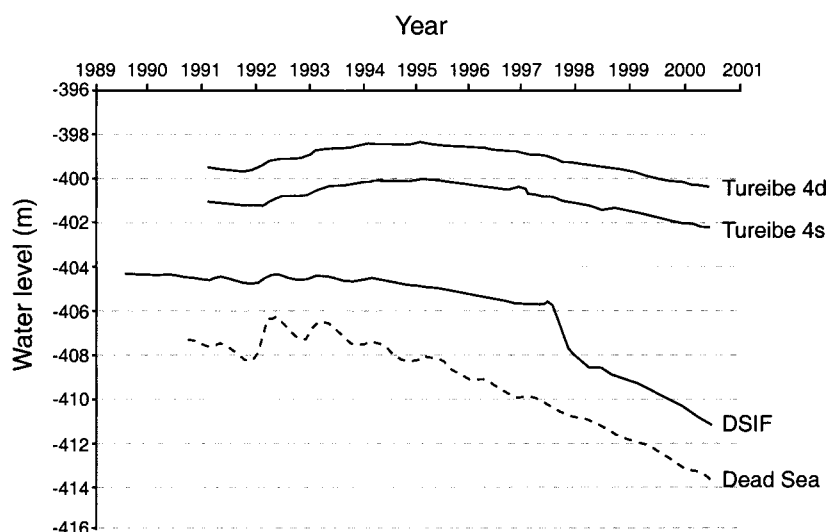
Year

Figure 2. Ground-water and Dead Sea levels for the period 1992–2000 (see Fig. 1 for well locations). Data retrieved every month. The abrupt water-level drop in DSIF well in 1997 is due to changes in the local hydrologic conditions (Y. Yechieli, 2001, personal commun.).
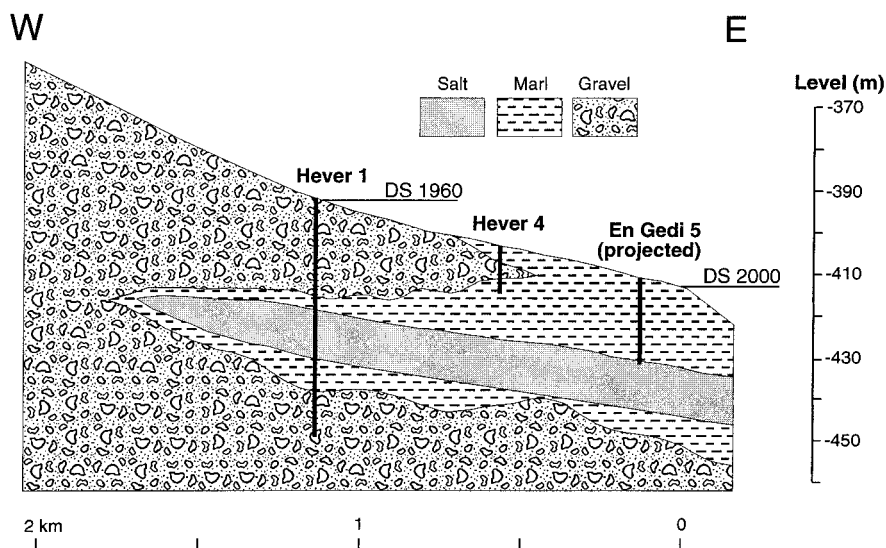

Figure 3. Schematic west-east cross section showing the subsurface structure in the Dead Sea coastal area (simplified after Wachs et al., 2000).

found at distances less than 1 km from the shore of the Dead Sea and are either clustered, distributed along straight lineaments, or aligned parallel to the Dead Sea shore (Itamar and Reizmann, 2000; Wachs et al., 2000). Two main types of gradual subsidence features have been observed in this region: (1) Some subsidence is restricted to an area as much as a few tens of meters wide around the sinkholes, often associated with concentric extensional cracks and crevices (Fig. 4A). Subsidence rates in such areas may reach 2 m/yr (E. Raz, 2000, personal commun.). These features are local and too small to be observed by InSAR (which can only resolve features >100 m across) and are thus excluded from further analysis. (2) Other subsidence features occupy large areas, up to a few square kilometers, that gradually subside. They may be identified in the field by small, internally drained basins and water ponds that formed after a substantial amount of subsidence had occurred (E. Raz, 2000, personal commun.). In places they are associated with small extensional cracks and fault escarpments (Fig. 4B). These features could be a result of one or more of the following mechanisms (see subsequent discussion): (1) dissolution of the

upper surface of the 20-m-deep salt layer (Fig. 3) by fresh water that flows above the salt, (2) aquifer-system consolidation due to the drop of the ground-water level (e.g., Tolman and Poland, 1940), and/or (3) structurally controlled or tectonic subsidence.

## INTERFEROMETRIC SYNTHETIC APERTURE RADAR (INSAR)

Method

Interferometric analysis of SAR images has become a widespread, valuable technique to measure subtle displacements at the ground surface (e.g., Gabriel et al., 1989; Massonnet and Feigl, 1998). When two radar scans are made at different times from almost the same viewing angle, a small change in the position of the target (ground surface) may create a detectable change in the phase of the reflected signals. The resulting difference of phase is expressed in an interference map (interferogram), in which the fringe pattern reflects the ground displacement that occurred between the two acquisitions; the product is referred to as a "change interferogram." Other factors, such as topography, orbital errors, and atmospheric delay, may also contribute to the resulting interferogram and are generally isolated and removed (see Appendix).

Each fringe cycle in a change interferogram corresponds to a contour of half the radar wavelength (28 mm in the case of European Remote Sensing [ERS] satellite data) satellite-to-ground line of sight (LOS) ground displacement. The mean incidence angle of ERS satellites is 23°; thus, in the case of pure vertical movement, one fringe cycle represents ~31 mm of displacement. To distinguish between horizontal and vertical displacements, we compared interferograms generated by the eastward-viewing ascending track orbits with those generated by the westward-viewing descending track orbits. Theoretically, an opposite color order in the interferograms of the two tracks indicates an opposite sense of displacement, suggesting predominance of horizontal displacements. A similar sense of LOS displacements implies either predominance of vertical displacement or horizontal displacement in the direction (i.e., north) bisecting the two tracks. For more details about the InSAR technique and its limitations, see the Appendix.

Data

SAR data for this study were collected by the European Space Agency Remote Sensing
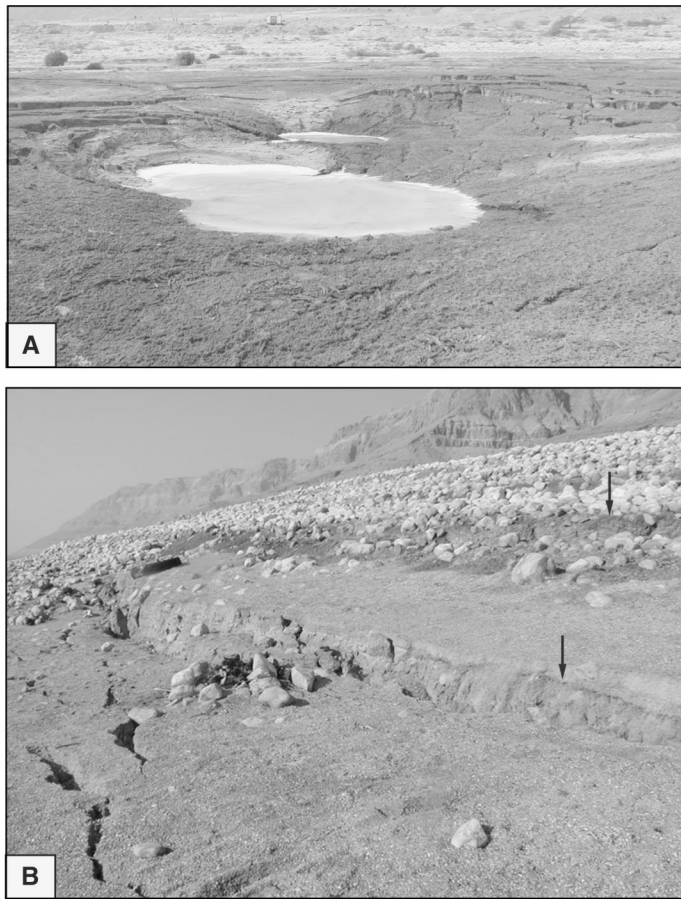
Figure 4. Photographs showing two types of gradual subsidence features. (A) Gradual subsidence in close vicinity to a sinkhole site east of En Gedi. Total subsidence is ~2 m and has occurred during a period of 2 yr. It is associated with concentric extensional cracks and crevices. (B) Subsidence associated with fault escarpments (arrows) and extensional cracks in the downfaulted, eastern (left) block, west of Mineral Beach sinkhole site.

Satellites ERS-1, which imaged the area between April 1992 and October 1997, and ERS-2, which has been imaging the area since July 1995. The normal orbital cycle for each satellite is 35 days. During the overlapping period (1995–1997), the two satellites performed tandem missions, at 1-day intervals. For this study we used 16 scenes from two SAR frames ~100 × 100 km each (Fig. 5): frame 621 (ascending track, 4 scenes) and frame 2979 (descending track, 12 scenes). Change (deformation) interferograms were generated for different time intervals of 2 to 71 months between 1992 and 1999 (Fig. 5).

Results

Several regions around documented sinkhole occurrences along the western shores of the Dead Sea and in the Lisan Peninsula were chosen for detailed interferometric analyses of uplift and subsidence (Fig. 1B). In the following sections, we describe the results by regions.

Western Dead Sea Shore

Figure 6 shows change interferograms for three subregions along the shore (Fig. 1B), spanning periods of 3 to 71 months between 1992 and 1999. Because the topography of the coastal area is almost flat and the topographic phase has been removed (see Appendix), the observed interferometric fringes are mostly due to surface deformation.

In all cases, the LOS displacements in a specific area are similar in the interferograms of the ascending and descending tracks (e.g., feature 1 in Fig. 6, B and D), suggesting that the InSAR-detected deformation is primarily due to vertical movements. A few circular and elongate subsidence features (depressions) are observed along and parallel to the shore. Most of these depressions appear in all the interferograms but with different magnitudes (Fig. 6).

For example, a circular depression, ~200 m wide, is seen at the tip of the Wadi Hever delta (marked 1 in Fig. 6, A–F). It is undetected in the interferogram that compares the area after three months ("3-month interferogram") (Fig. 6A), but shows about one fringe cycle (31 mm) in the 24-month interferogram (Fig. 6B) and more than 1.5 fringe cycles (~50 mm) in the 71-month interferogram (Fig. 6F). In the Hever sinkhole site (marked 2 in Fig. 6, A–C), subsidence is ~10 mm in the 3-month interferogram (Fig. 6A) and grows gradually to a maximum value of 30 mm in the 64-month interferogram (Fig. 6C). In the area surrounding the Zerruya sinkhole site (marked 3 in Fig. 6, D–F), subsidence increases from 10 to 45 mm for the 20- to 71-month interferograms, respectively. The subsiding area is ~3 × 1 km, with its long dimension roughly parallel to the coast. It is detected in the field by the internally drained ponds at its center. In the Mineral Beach site (marked 4 in Fig. 6, G–I), the subsidence (~30 mm) is similar in the 24-, 44-, and 71-month interferograms. Here, only the dimensions of the subsiding areas change with time. The three isolated depressions observed in the 24-month interferogram (Fig. 6G) interconnect and become an elongate, shore-parallel depression in the longer-term interferograms (Fig. 6, H and I). The subsiding area is bounded on the west by small fault escarpments (Fig. 4B).

End Brines' Outlet Channel

The outlet channel of the Dead Sea end brines (Fig. 1B) drains the end brines from the Dead Sea Works evaporation ponds back to the northern basin of the Dead Sea. Short-term interferograms of 3 and 15 months show a high rate of deformation in that area. The 3-month interferogram from 1995 (Fig. 7A) shows a north-trending depression of about one cycle (30 mm), whereas 15-month interferograms of 1995–1997 (Fig. 7B) and 1997–1999 show irregular subsidence patterns of almost three fringe cycles (80 mm). The subsiding area is bounded in the southeast by a northeast-striking lineament (Fig. 7B), suspected as the surface expression of a fault (Bartov, 1999). Abundant sinkholes have been forming in this area since at least 1982 (Itamar and Reizmann, 2000) and the ground surface is rapidly changing, as observed by the decorrelation in all interferograms that span more than 15 months (Fig. 7, C and D).

The Lisan Peninsula

The Lisan Peninsula, overlying a salt diapir, is built mostly of the late Pleistocene Lisan Formation; the margins of the peninsula con-

Frame 621

A

Frame 2979

B
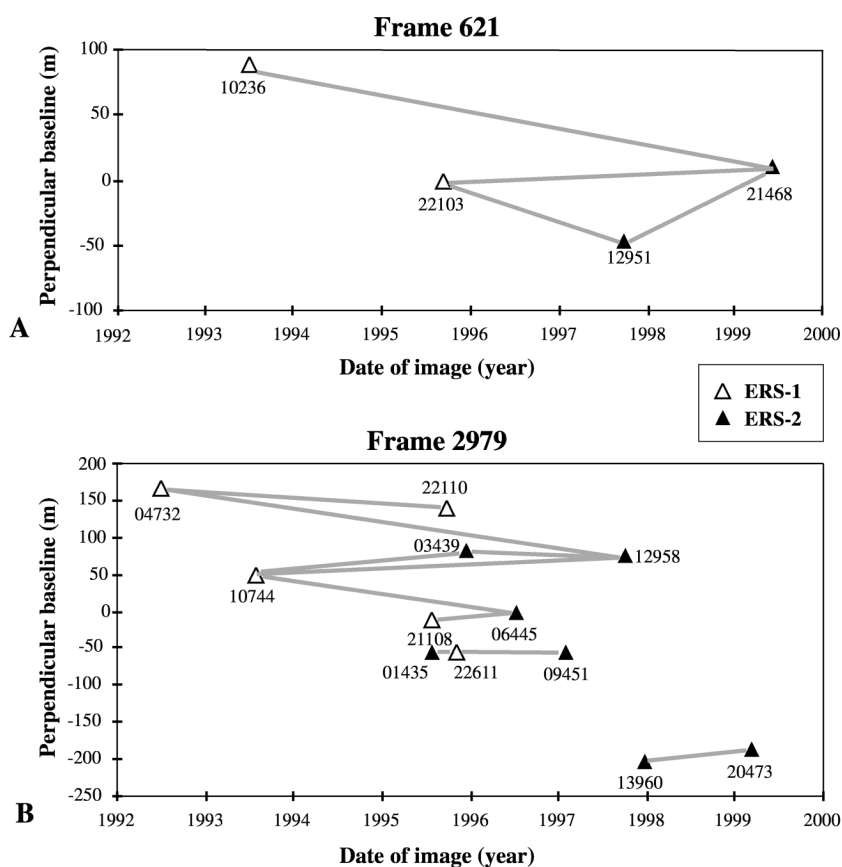
Figure 5. Orbits and perpendicular baselines chosen for this study. In each frame, baselines are measured relative to a master image of zero baseline. Pairs used for change interferograms are connected by gray lines. (A) Frame 621 (ascending track). (B) Frame 2979 (descending track).

sist of the Holocene Ze'elim Formation (Bartov, 1999). The salt diapir is elongated in the north-south direction (Fig. 1B) and includes several subdomes and one structural depression (Bartov, 1999). Folds in the Lisan Formation layers above the diapir delineate the structures of the subdomes. Two faults, striking north and northeast, bound the peninsula in the east and northwest, respectively (Bartov, 1999). At the southeastern side of the peninsula, in Ghor Al Haditha (Fig. 1B), subsidence and sinkhole formation date back to the 1960s (Swarieh et al., 2000); they are causing serious damage and are a threat to farmers.

Diverse uplift and subsidence features are seen in the peninsula and in the adjacent shores of the Dead Sea (Figs. 7, 8). These are detailed next.

Coastal Subsidence. The Lisan Peninsula is surrounded by a subsiding coast. Coastal subsidence includes circular (marked 1 in Fig. 7) and coast-parallel, elongated depressions (2 in Fig. 7), showing phase differences that cor-

respond to maximum subsidence of ~80 mm in the 50-month pair (Fig. 7D). The amount of subsidence correlates with the time span of each interferogram (Figs. 7, 9). In the sinkhole area of Ghor Al Haditha, subsidence of ~30 mm has been observed in the 3-month interferogram (marked 3 in Fig. 7A). Because it is populated and cultivated, longer-period interferograms of this area are decorrelated (Fig. 7, B–D).

Subsidence in an Ancient Alluvial Fan. An ancient alluvial fan is elevated by ~100 m above the Dead Sea coastal plain east of Ghor Al Haditha (Fig. 1B). An elliptical WSSF (marked 4 in Fig. 7, B–D), ~3 × 2 km in size, with maximum subsidence of 45 mm in an 18-month interferogram, is detected in some interferograms of this area, but is undetected in others (see Discussion).

Subsidence Above Salt-Dome Margins. A few curvilinear shallow depressions are found above the presumed margins of the salt domes in the southern part of the peninsula in all interferograms that exceed 12-month time inter-

vals (marked 5 in Fig. 7, B and C; Fig. 8). The amount of subsidence in these features is proportional to the period spanned by the interferogram, ranging from 10 to 55 mm in the 12- to 71-month interferograms, respectively (Fig. 9).

Uplift. Elevation changes in Lisan Formation units that were uplifted by the diapir suggest a long-term 1–2 mm/yr average uplift rate of the Lisan diapir (Bartov, 1999). Our change interferograms show no sign of uplift in the southern or central domes where the diapir is closest to the surface. Possible evidence for uplift is seen in the northern part of the peninsula (marked 6 in Fig. 7, C and D). Here, ~10 mm and 20 mm of uplift are observed in the 22- and 50-month interferograms, respectively, suggesting an average uplift rate of ~4–5 mm/yr.

DISCUSSION

Subsidence Rates

Subsidence rates were calculated from different time-interval interferograms (Fig. 9). Rates ranged between 5 mm/yr (Hever sinkhole site) and ~20 mm/yr in (northern part of the Lisan Peninsula). Extremely high rates of >60 mm/yr were found in the end brines' outlet channel and in the Ghor Al Haditha sinkhole site. In several sites (Hever, Zerruya, Lisan NE, and Lisan S trenches; Fig. 9), the subsidence rate was fairly constant. On the other hand, other patterns of long-term behavior were also common. At the Hever delta, the amount of subsidence increased with time to a maximum of 45 mm in a 20-month pair but did not continue increasing beyond that time (Fig. 9). At the Mineral Beach site, long-term interferograms did not show more subsidence than short-term interferograms (Fig. 6, G–I).

Subsidence rates in the alluvial fan east of Ghor Al Haditha are entirely noncorrelated with the time interval spanned by the interferograms (Figs. 7, 9). An 18-month pair of 1995–1997 shows the highest subsidence of 45 mm, whereas longer-period interferograms of 64 months (1992–1997) and 71 months (1993–1999) that include the 1995–1997 period show subsidence of only 25 mm and 10 mm, respectively. No subsidence is found in the 1992–1995 and 1997–1999 interferograms (Fig. 9). To explain this anomaly, we first confirm that the interferograms show true deformation and do not express topographic or atmospheric effects. The topographic effect is excluded by the lack of correlation between the number of fringes in this feature (that correspond to the amount of deformation) and the

perpendicular baseline of the respective interferogram (see Fig. 5). For example, deformation of 40 mm is observed in pair 22611_09451 (Fig. 7B) with 1 m perpendicular baseline (Fig. 5), whereas 20 mm deformation is observed in pair 10744_06445 (Fig. 7D) with 50 m perpendicular baseline (Fig. 5). An error due to atmospheric propagation delay is also unlikely because high fringe rates are observed in several unrelated pairs of different times.

Comparing the subsidence with the actual acquisition dates of the interferograms for the alluvial fan east of Ghor Al Haditha (Fig. 10) reveals that the highest subsidence rates are found in the 1995–1997 interferograms, whereas no subsidence is found in the 1992–1995 and 1997–1999 interferograms. This result could imply that subsidence was due to ground movements during (or following) a certain event in the 1995–1997 period, and the rate of the subsidence decreased shortly afterward. A possible trigger for instantaneous subsidence in that period could be the 22 November 1995 $M_w = 7.1$ Nuweiba earthquake in the Gulf of Elat, ~300 km south of the Dead Sea (e.g., Baer et al., 1999). This earthquake affected ground-water levels at distances of more than 400 km away from the epicenter (Y. Yechieli, 2001, personal commun.) and caused damage to the water system leading to the citadel of Shawbak (Jordan), 80 km south of the Lisan Peninsula (A. Salameh, 1999, personal commun.).

Temporal and Spatial Relationships Between Sinkholes and Subsidence

Many sinkhole sites along the Dead Sea shoreline are found in association with gradual subsidence. However, although InSAR observations show that large sections of the shore are subsiding (e.g., the entire shore of the Lisan Peninsula), sinkholes are generally localized in distinct areas (Fig. 1B). In some of these areas, gradual land subsidence has been observed around sinkholes a short time after they formed (Fig. 4A; Wachs et al., 2000). Opposite relationships—i.e., local or regional subsidence that developed into sinkholes— were not observed in the field. In one area that includes the Zerruya sinkhole site, however, InSAR observations show regional subsidence between 1995 and 1997 (Fig. 6D), whereas sinkholes were first observed in 1999 (Itamar and Reizmann, 2000). This place is the only one so far where observed regional subsidence predated sinkhole formation. Because all other sites formed before SAR data were available, the possibility for similar relationships elsewhere could not be examined, but may be evident in new sinkhole occurrences in the future.

Geologic and Mechanical Constraints on the Subsidence Mechanism

Wide, shallow subsidence features (WSSFs) are formed mainly at short distances, less than 0.5 km, from the shoreline of the Dead Sea. Borehole data (Wachs et al., 2000) show that the subsurface in these subsiding areas is dominated by marl and salt, with gravel beneath (Fig. 3). West of this strip that shows subsidence, to a distance of ~1.5 km from the shoreline, the salt layer is overlain by alternating coarse- and fine-grained clastic material; the abundance of coarse material increases westward. No gradual subsidence has been found in this region. Under conditions of dropping ground-water levels, enhanced salt dissolution is expected to occur in the west rather than close to the shoreline (because when the Dead Sea–freshwater interface migrates eastward, it first exposes the western side to fresh water). We thus exclude salt dissolution as a dominant subsidence mechanism in these nearshore areas.

To further explore the aquifer-system compaction mechanism, we now analyze the relationships between changes in water levels and deformation of the aquifer system. The process, described by the aquitard-drainage model (Terzaghi, 1925; Tolman and Poland, 1940), is well known from water-extracted regions worldwide (e.g., Ireland et al., 1984; Poland and Ireland, 1988). A drop of ground-water level results in the decrease of pore pressure in the aquifer system. Consequently, the effective stress (overburden minus pore pressure) increases (Terzaghi, 1925), the pore structure in the fine-grained marl layers is rearranged to decrease pore space, and the layers may consolidate and collapse, resulting in land subsidence. The location of WSSFs along the Dead Sea shores and the amount of subsidence are thus expected to be a measure of the relative abundance of marl in the subsurface.

In the following, we show the expected amount of subsidence caused by the collapse of marl units of different thickness in the subsurface, corresponding to changes in the distance from the shoreline (Fig. 3). The calculated subsidence is then compared to the InSAR-observed subsidence. Calculations were conducted for marl layers with thicknesses of 5, 10, and 15 m, located between granular materials, in which the roof of each marl layer lies 10 m below ground surface.

Water level was assumed to be initially at ground surface and to drop according to the levels indicated for water well Dead Sea interface (DSIF) in Figure 2. This water-level change was approximated by a bilinear variation—a drop rate of 0.4 m/yr from 1992 until 1997 and a drop rate of 1.2 m/yr from 1997 until 2001. The analysis was carried out by assuming the relevant yearly drop to occur instantaneously at the beginning of each year and then allowing the marl layer to undergo a process of consolidation during the year, until the next drop. In order to simulate instantaneous water drop at the beginning of the first year, the unit weight of the top 0.4 m of the soil profile was assumed to increase instantaneously by the unit weight of the salt water, resulting in a stress increment throughout the profile of ~5 kPa. This process was repeated at the beginning of each year. From 1997, when water drop increased to 1.2 m/yr, a stress increment of 14 kPa was applied each year.

One-dimensional (vertical) consolidation was assumed according to Terzaghi's theory (Terzaghi, 1925), as is common in standard soil mechanics computations. Soil parameters were based on data obtained from the soil mechanics laboratory of the Israel Institute of Technology (Technion), from tests performed on undisturbed samples from the Ein Boqeq area (~15 km south of DSIF well). The marl-consolidation coefficient, c_v, was taken as 10^{-2} cm^2/s, associated with a coefficient of permeability of ~10^{-3} m/day. The marl was assumed to be normally consolidated, with a compression index, c_c in the range 0.1–0.2. The initial void ratio of the marl is of the order of 1.0.

According to Terzaghi's consolidation theory, the time (t) required to complete 90% consolidation is given by

$$t = 0.848(H/2)^2/(c_v),$$

where H is the thickness of the marl layer.

The calculations show that due to the relatively high value of the marl-consolidation coefficient, consolidation was completed relatively quickly, within the year following the instantaneous water-level drop; therefore, there was no superposition of time effects from one year to the next.

The settlement δ resulting from consolidation of the marl layer may be found from the expression

$$\delta = [H/(1 + e)] \times c_c \log(\sigma_f/\sigma_0),$$

where e is the void ratio, σ_f is the final vertical effective stress in the marl layer following
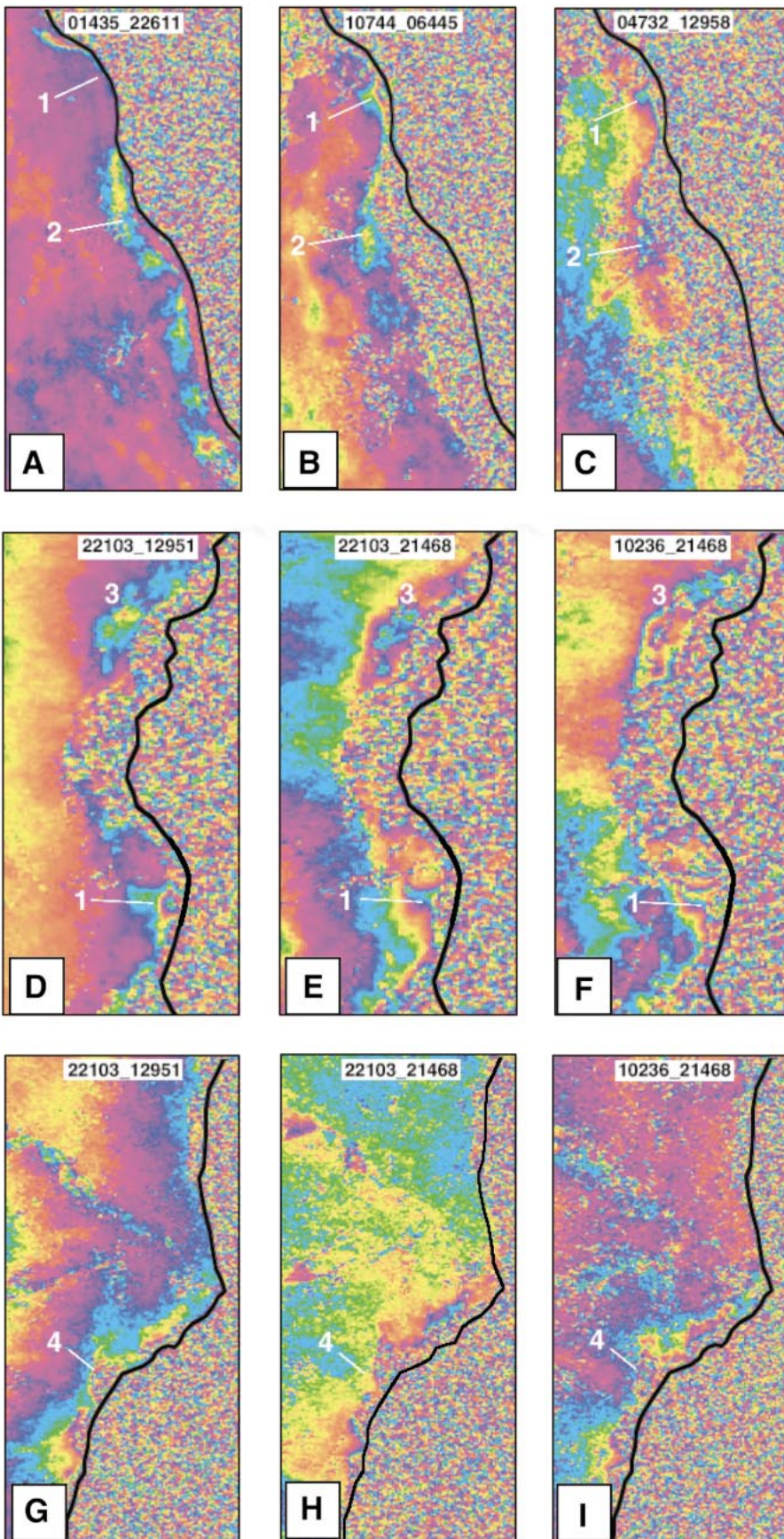
Figure 6. Change interferograms for three areas along the western shore of the Dead Sea (see Fig. 1B for locations). Solid lines represent the 1995 coastline; the pattern of fine colored pixels is water. Interferograms A–C show the area south of Wadi Hever (frame 2979, descending track) for periods of 3, 35, and 64 months, respectively. Hever delta and Hever sinkhole site are marked 1 and 2, respectively. Width of image represents 3.5 km. Interferograms D–F show the area south of En Gedi (frame 621, ascending track) for periods of 24, 44, and 71 months, respectively. Zerruya sinkhole site and Hever delta are marked 3 and 1, respectively. Width of image represents 3.5 km. Interferograms G–I show the area surrounding Mineral Beach sinkhole site (marked 4), for periods of 24, 44, and 71 months. Width of image represents 1 km. Frame 621, ascending track.

loading, and σ_0 is the initial effective stress prior to loading.

Figure 11 shows development of subsidence for the different marl layers, assuming a value of $c_c = 0.1$; for higher values of c_c, the subsidence would be expected to increase linearly. The InSAR subsidence measurements in three areas during the years 1992–1999 are shown for comparison. Both InSAR measurements and the calculated subsidence include some uncertainty, however, as a first approximation, our results show that the calculations predict subsidence values in the order of the measured subsidence, which is by itself a support of the compaction model. Furthermore, the Hever site, which is the farthest away from the Dead Sea shores ($\sim$500 m), shows the lowest rate of subsidence, in agreement with the prediction of a thinner marl layer (Fig. 3). The Lisan northeast site, with the highest subsidence rate, is located right at the Dead Sea shoreline (Fig. 1). Subsidence measurements in this site suggest a marl layer thicker than 20 m.

Structurally Controlled Subsidence

The coast-parallel fault escarpments and extensional cracks (Fig. 4B) and the northeast-striking lineament along the southeastern side of the WSSF along the end brines' outlet channel suggest that certain areas have subsided along faults or other structural elements. The fault escarpments and extensional cracks resemble in appearance surface expressions of landslides, in this case, seaward landslides that respond to the deepening of
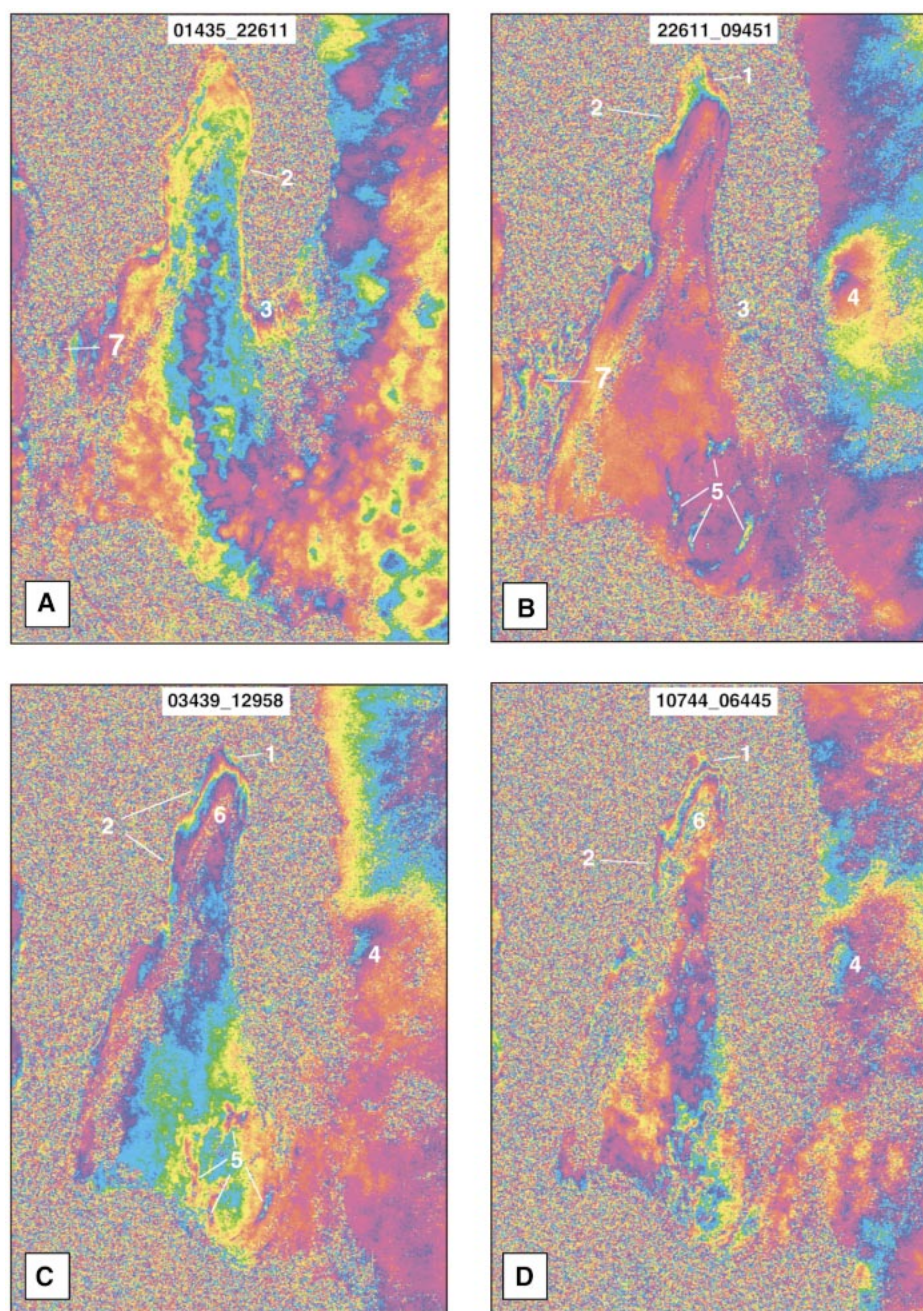
Figure 7. Change interferograms for the Lisan Peninsula and the adjacent Dead Sea shore; location in Figure 1B. All image widths represent 20 km. Periods between acquisition: (A) 3 months, (B) 15 months, (C) 22 months, (D) 50 months. Locations and features shown by numbers: 1—circular coastal depressions, 2—elongated coastal depressions, 3—Ghor Al Haditha sinkhole site, 4—Alluvial fan, east of Ghor Al Haditha, 5—trenches and depressions above salt-dome margins, 6—uplift at the northern part of the peninsula. 7—End brines' outlet channel.
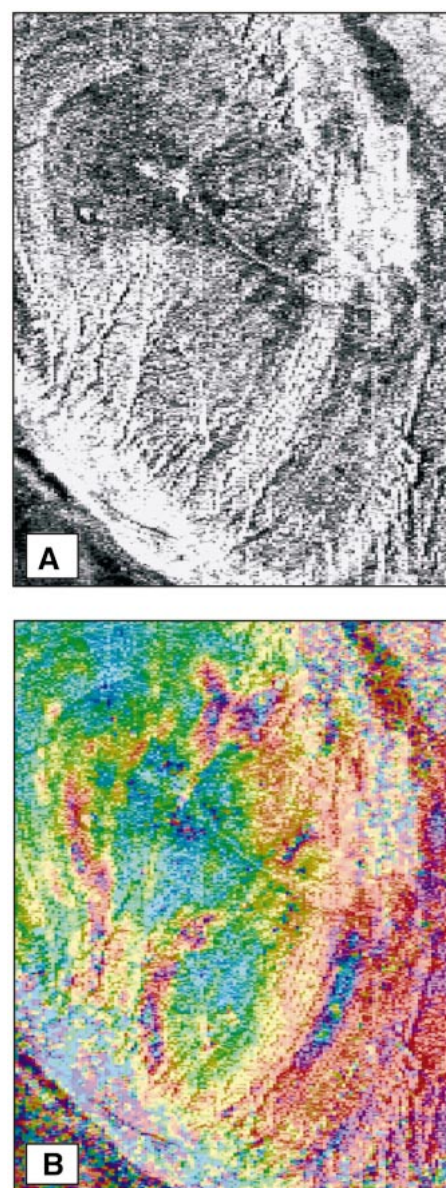

Figure 8. (A) An amplitude image of the southern salt dome, Lisan Peninsula. (B) Superposition of the amplitude image and a 22-month interferogram (southern part of Fig. 7C). Note the correlation between subsidence (curvilinear trenches) and specific layers above the margins of the dome. Width of image is 6 km.

the northern basin of the Dead Sea. The lineament that bounds subsidence along the end brines' outlet channel has been suggested as a fault by Bartov (1999) but has not shown any signs of activity (such as seismicity) in recent years (Anonymous, 2001). This fact precludes tectonic creep as an explanation to the subsidence. The fault, however, may separate units with different mechanical properties, thus enhancing differential subsidence on its more compressible, northwestern side. Fault-bounded subsidence has also been de-

scribed in the Las Vegas (Nevada, USA) region (Amelung et al., 1999).

The curvilinear depressions observed in the southern part of the Lisan Peninsula are different in extent and geometry. They are also structurally controlled, following specific layers above the margins of the domes (Fig. 8). Their formation may be caused by one or more of the following mechanisms: (1) en-
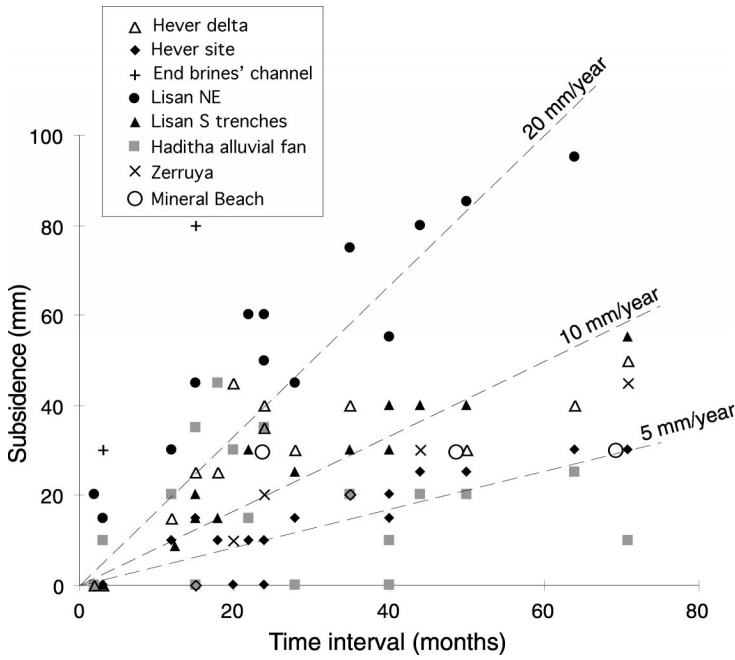
Figure 9. Subsidence values for the studied areas as measured by different time-interval interferograms. Dashed lines indicate 5, 10, and 20 mm/yr rates.

hanced mass-removal or dissolution in a specific layer due to its composition (e.g., rich in marl or salt), (2) collapse within a layer that underwent enhanced extension at the margin of the dome, and/or (3) dissolution of salt at the margins of the salt dome at depths of 100–250 m.

SUMMARY AND CONCLUSIONS

We applied InSAR measurements to map and calculate rates of vertical displacement phenomena in the Dead Sea basin. Sixteen SAR scenes acquired during a 7 yr period (1992–1999) were used to characterize the main occurrences of subsidence and uplift in this area. To relate subsidence features to the documented sinkholes, we chose several regions of sinkhole occurrences along the Dead Sea for detailed interferometric analysis. Our change interferograms span periods of 2 to 71 months. Circular and elongate features are observed along the Dead Sea shore, showing phase differences that correspond to subsidence rates ranging between 5 mm/yr and 20 mm/yr. In the outlet channel of the Dead Sea
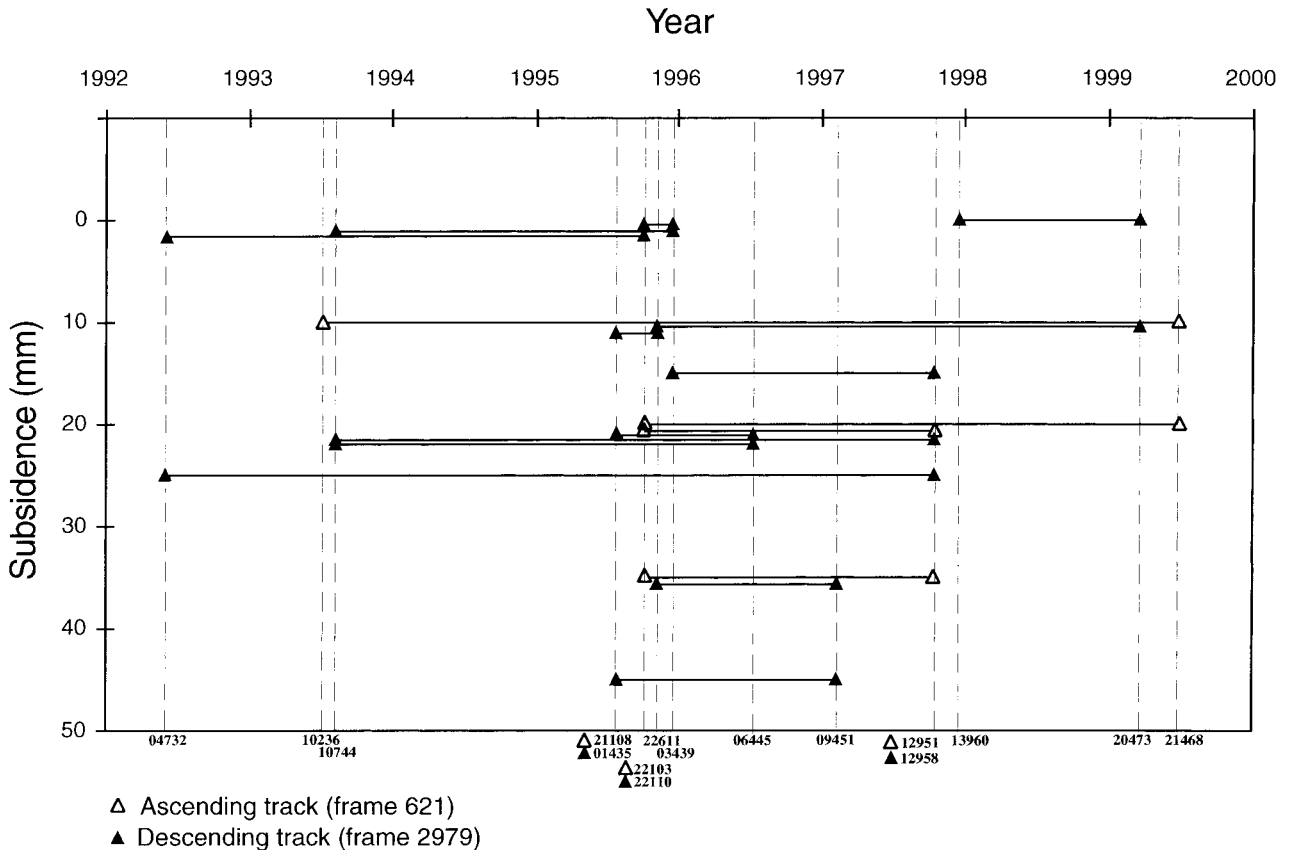

Figure 10. Subsidence plotted against the actual acquisition dates of the interferometric pairs in the ancient alluvial fan east of Ghor Al Haditha. The small numbers at the bottom of the plot mark the orbit numbers (see Fig. 5).

end brines (Israel and Jordan) and in the Ghor Al Haditha sinkhole area (Jordan), the rate may reach values higher than 60 mm/yr. Diverse uplift and subsidence features were observed, including coastal subsidence, subsidence in ancient alluvial fans, and subsidence above salt-dome margins. During the period that is covered by the interferograms, the level of the coastal ground water has dropped by ~6 m. The combination of this water-level drop with an aquifer that overlies fine-grained marly material provides appropriate conditions for gradual subsidence by aquifer-system consolidation. In certain areas, subsidence appears to be structurally controlled by faults, seaward landslides, and salt domes. Calculations of the expected aquifer-system consolidation and comparison with InSAR observations confirm that the observed subsidence along the Dead Sea shores occurred where the total thickness of the fine-grained marl layers is between 5 m and 20 m in the upper 30 m below the surface.

Our InSAR observations show subsidence in areas that are considerably wider than the sinkhole sites. WSSFs are thus unlikely to be directly related to the sinkholes and cannot serve as predictable precursors to sinkhole development. We do, however, consider that InSAR subsidence monitoring should be continued in order to serve as a comparison with findings of future sinkhole development for the determination of possible circumstantial relationships between the two features. Finally, our study has shown that considerable parts of the Dead Sea shores are vulnerable to subsidence. This result emphasizes the environmental implications of these features and the care that should be taken in any future land-use planning in this area.

APPENDIX

We use radar imagery collected by the C-band (5.2 GHz) synthetic aperture radar (SAR) aboard the ERS-1 and ERS-2 satellites. The raw SAR data are processed using a JPL-heritage (i.e., Jet Propulsion Laboratory) SAR processor. The output signal is a measure of the complex backscatter of a patch on the ground delayed by the travel time of the radar waves from sensor to target and back (see Curlander and McDonough, 1991). The basic steps of our interferometric SAR (InSAR) data processing (Scripps Institution of Oceanography SAR processing system—SIOSAR) are quite standard. We focus the raw radar echoes to SAR images and match the images to a subpixel level. We then form an interferogram by multiplying each complex pixel in one image by the complex conjugate of the matching pixel in the other image. The phase of the interferogram consists of a number of components as shown in Appendix Table A1. Precise orbital information (Scharroo and Visser, 1998), with respect to the WGS84 ellipse and EGM96 ellipsoid, is used to
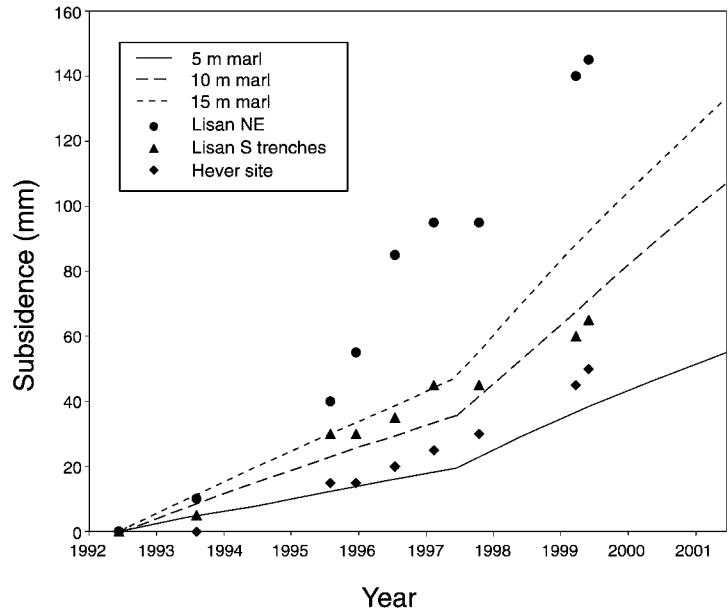

Figure 11. Calculated subsidence assuming one-dimensional (vertical) consolidation (Terzaghi, 1925) above marl layers 5, 10, and 15 m thick, as labeled. Parameters for the calculations include average water-level drops in DSIF well for the years 1992–1997 and 1997–2001 (see Fig. 2) and soil parameters based on tests of undisturbed samples from the En Boqeq area (Fig. 1). InSAR measurements of subsidence in three areas, (Lisan NE, Lisan S trenches, and Hever site) during the years 1992–1999 are shown for comparison. See text for further discussion.

TABLE A1. CONTRIBUTIONS TO INTERFEROMETRIC PHASE

Phase component	Length scale	Knowledge to remove	Scientific importance
Earth curvature*	Ellipsoid (WGS84)	Known	
Topography[†]	Broad spectrum	Known at long λ	Foundation for all fields[§]
Surface deformation[#]	Broad spectrum	Unknown	Geology, geophysics, glaciology, etc.[**]
Orbit error[††]	Almost a plane	Unknown	
Ionospheric delay[§§]	Red spectrum	Long λ known from GPS	Ionospheric studies
Tropospheric delay[##]	Power law	Unknown	Atmospheric studies
Phase noise[***]	White spectrum	Unknown	

*Joughin et al. (1996).
[†]Zebker and Goldstein (1986); Zebker et al. (1994a); Jakowatz et al. (1996).
[§]Evans et al. (1995); Burke and Dixon (1988).
[#]Massonnet et al. (1993); Zebker et al. (1994b); Peltzer et al. (1996).
[**]Massonnet and Feigl (1998); Dixon et al. (1995).
[††]Massonnet and Rabaute (1993).
[§§]Curlander and McDonough (1991).
[##]Rosen et al. (1996); Hanssen et al. (1999).
[***]Li and Goldstein (1990).

remove the largest phase signal due to Earth curvature. A low-resolution digital elevation model (DEM) is projected into the radar coordinates and removed from the full-resolution interferogram. Because precise orbits are available, one three-dimensional ground control point is sufficient to solve for the range bias and the along-track shift due to the nonzero Doppler shift of the radar footprint (i.e., spacecraft yaw error). In addition to removing the crude DEM, the residual phase from a suitable tandem ERS-1 to ERS-2 pair is unwrapped and added back to the crude topographic phase model to form a full-resolution topography model needed for isolating the phase signal due to ground motion. This hybrid approach of topographic phase construction retains the long-wavelength accuracy of the two-

pass method (Massonnet and Feigl, 1998) and the full topographic resolution of the four-pass method (Zebker et al., 1994a).

There are several data-processing steps that are either done differently in SIOSAR or should be elaborated upon for the sake of explaining the resolution and interpretation of our results. These include estimation of baselines from orbital knowledge, image filtering, and phase-gradient computation and combination.

Use of Precise Orbital Information

In contrast to previous studies, which estimated baseline parameters from imagery, topography data, and perhaps known ground control points, we com-

pute baselines from ERS-1 and ERS-2 precise orbits provided by Scharroo and Visser (1998). These orbits have radial accuracy of 50 mm and cross-over repeatability within 70 mm, giving an overall baseline accuracy better than 70 mm. The advantage of this approach is that surface displacements and long-wavelength atmospheric artifacts are not absorbed into the baseline estimate. Repeat orbits are usually not parallel, necessitating the computation of a new baseline at every point in both azimuth and range within an image frame (e.g., Gabriel and Goldstein, 1988).

Interferogram Filtering

Methods of filtering interferograms range from simple averaging over pixels (taking looks) (e.g., Gabriel et al., 1989), to spatially variable filters whose power spectra are matched to that of the local phase (Goldstein et al., 1988; Werner et al., 1992). We filtered the real and imaginary parts of the complex interferogram (with pixel spacing as sampled by the radar) separately using a low-pass Gaussian 5 point by 17 point filter, which has a 0.5 gain at a wavelength of 200 m (Sandwell and Price, 1998). Although the Gaussian filter operation takes substantially more computer time than the standard five-look average followed by decimation, it avoids the problem of folding the noise from the first sidelobe of the boxcar (multilook) filter back into longer wavelengths where it lowers the coherence. This issue is more important for phase-gradient estimation than it is for standard interferometric phase recovery.

Effects of propagation medium on range delay

Because we cannot yet remove the atmospheric signal from the topographic phase-corrected interferograms, it is important to be able to recognize atmospheric artifacts so that they are not confused with deformation. Short-wavelength atmospheric artifacts (which could be confused with small-scale tectonic deformations) typically have length scales on the order of 5–10 km and can cause as much as 6 cm of excess two-way path length (two interferogram fringes). Examples can be found in Massonnet and Feigl (1995), Rosen et al. (1996), Zebker et al. (1997), and Hanssen (2001). Interferograms showing obvious atmospheric contamination are discarded.

Regional atmospheric effects corresponding to long-wavelength, ionospheric perturbations and to differences in the hydrostatic component of the troposphere manifest themselves as a planar phase trend in an interferogram (Tarayre and Massonnet, 1996). This phase trend makes it necessary either to compute an "artificial baseline" (Tarayre and Massonnet, 1996) or to remove the long-wavelength atmospheric effect from the interferogram at some point in the data processing. If these regional effects are not removed, they will produce a constant offset in the phase-gradient map, which could be interpreted as a regional tilt.

ACKNOWLEDGMENTS

REFERENCES CITED

Amelung, F., Galloway, D.L., Bell, J.W., Zebker, H.A., and Laczniak, R.J., 1999, Sensing the ups and downs of Las Vegas: InSAR reveals structural control of land subsidence and aquifer-system deformation: Geology, v. 27, p. 483–486.

Anonymous, 2001, Earthquakes in and around Israel, 1907–2001: Lod, Geophysical Institute of Israel, CD-ROM.

Arkin, Y., and Gilat, A., 2000, Dead Sea sinkholes—An ever-developing hazard: Environmental Geology, v. 39, p. 711–722.

Baer, G., Sandwell, D., Williams, S., Shamir, G., and Bock, Y., 1999, Coseismic deformation associated with the November 1995, $M_w = 7.1$ Nuweiba earthquake, Gulf of Elat (Aqaba), detected by synthetic aperture radar interferometry: Journal of Geophysical Research, v. 104, p. 25221–25232.

Bartov, Y., 1999, The geology of the Lisan Formation in Massada plain and the Lisan Peninsula [M.Sc. thesis]: Jerusalem, Hebrew University, 63 p. (in Hebrew, English abstract).

Bartov, Y., Sneh, A., Fleischer, L., Arad, V., and Rosensaft, M., 2000, Map of potentially active faults in Israel: Geological Survey of Israel Report GSI/23/2000, 28 p.

Begin, B.Z., Ehrlich, A., and Nathan, Y., 1974, Lake Lisan—The Pleistocene precursor of the Dead Sea: Geological Survey of Israel Bulletin 63, 30 p.

Burke, K., and Dixon, T.H., 1988, Topographic Science Working Group to the Land Processes Branch, Earth Science and Applications Division: Houston, Texas, National Aeronautics and Space Administration Lunar and Planetary Sciences Institute, Report, 64 p.

Carbognin, L., Gambolati, G., and Johnson, A.I., eds., 2000, Land subsidence: Ravenna, Italy, Proceedings of the Sixth International Symposium on Land Subsidence.

Curlander, J.C., and McDonough, R.N., 1991, Synthetic aperture radar: Systems and signal processing: New York, John Wiley and Sons, Inc., 647 p.

Dixon, T.H. et al., 1995, SAR interferometry and surface change detection, Report of a workshop held on Boulder, Colorado, February 3–4, 1994: University of Miami, Rosenstiel School of Marine and Atmospheric Sciences, Report RASMAS TR 95-003, 97 p.

Evans, D.L., Apel, J., Arvidson, R., Bindschadler, R., Carsey, F., Dozier, J., Jezek, K., Kasischke, E., Li, F., Melack, J., Minster, B., Mouginis-mark, P., and van Zyl, J., 1995, Spaceborne synthetic aperture radar: Current status and future directions, A report to the Committee on Earth Sciences Space Studies Board, National Research Council: Washington, D.C., National Aeronautics and Space Administration Technical Memorandum 4679, 197 p.

Fielding, E.J., Blom, R.G., and Goldstein, R.M., 1998, Rapid subsidence over oil fields measured by SAR interferometry: Geophysical Research Letters, v. 25, p. 3215–3218.

Gabriel, A.K., and Goldstein, R.M., 1988, Crossed orbit interferometry: Theory and experimental results from SIR-B: International Journal of Remote Sensing, v. 9, p. 857–872.

Gabriel, A.K., Goldstein, R.M., and Zebker, H.A., 1989, Mapping small elevation changes over large areas: Differential radar interferometry: Journal of Geophysical Research, v. 94, p. 9183–9191.

Galloway, D.L., Hudnut, K.W., Ingebristen, S.E., Phillips, S.P., Peltzer, G., Rogez, F., and Rosen, P.A., 1998, Detection of aquifer system compaction and land subsidence using interferometric synthetic aperture radar, Antelope Valley, Mojave Desert, California: Water Resources Research, v. 34, p. 2573–2585.

Galloway, D.L., Jones, D.R., and Ingebristen, S.E., eds., 1999, Land subsidence in the United States: U.S. Geological Survey Circular 1182, 177 p.

Goldstein, R.M., Zebker, H.A., and Werner, C.L., 1988, Satellite radar interferometry: Two-dimensional phase unwrapping: Radio Science, v. 23, p. 713–720.

Hanssen, R., 2001, Radar interferometry: Data interpretation and error analysis [Ph.D thesis]: Delft, Netherlands, Delft University of Technology, 308 p.

Hanssen, R.F., Weckwerth, H.A., Zebker, H.A., and Klees, R., 1999, High-resolution water vapor mapping from interferometric radar measurements: Science, v. 283, p. 1297–1299.

Ireland, R.L., Poland, J.F., and Riley, F.S., 1984, Land subsidence in the San Joaquin Valley, California, as of 1980: U.S Geological Survey Professional Paper 437-I, 93 p.

Itamar, A., and Reizmann, Y., 2000, Air photo survey of sinkholes in the Dead Sea area: Geological Survey of Israel Current Research, v. 12, p. 21–24.

Jakowatz, C.V., Wahl, D.E., Eichel, P.H., Ghiglia, D.C., and Thompson, P.A., 1996, Spotlight-mode synthetic aperture radar: A signal processing approach: Boston, Kluwer Academic Publishers, 429 p.

Joughin, I., Winebrenner, M., Fahnestock, R., Kwok, R., and Krabill, W., 1996, Measurement of ice sheet topography using satellite-radar interferometry, Journal of Glaciology, v. 42, p. 10–22.

Klein, C., 1985, Fluctuation of the levels of the Dead Sea and climatic fluctuation in the country during historical times: Jerusalem, International Symposium on Scientific Basis for Water Resources Management, September 19–23: Additional Paper and Posters Summaries, v. 2, p. 197–224.

Li, F.K., and Goldstein, R.M., 1990, Studies of multibaseline spaceborne interferometric synthetic aperture radar: IEEE Transactions on Geoscience and Remote Sensing, v. 28, p. 88–97.

Massonnet, D., and Feigl, K., 1995, Discriminating geophysical phenomena in satellite radar interferograms: Geophysical Research Letters, v. 22, p. 1537–1540.

Massonnet, D., and Feigl, K., 1998, Radar interferometry and its application to changes in the Earth's surface: Reviews of Geophysics, v. 36, p. 441–500.

Massonnet, D., and Rabaute, T., 1993, Radar interferometry: Limits and potential: IEEE Transactions on Geoscience and Remote Sensing, v. 31, p. 455–464.

Massonnet, D., Rossi, M., Carmona, C., Adragna, F., Peltzer, G., Feigl, K., and Rabaute T., 1993, The displacement field of the Landers earthquake mapped by radar interferometry: Nature, v. 364, p. 138–142.

Neev, D., and Hall, J.H., 1979, Geophysical investigation of the Dead Sea: Sedimentary Geology, v. 23, p. 209–238.

Peltzer, G., Rosen, P., Roges, F., and Hudnut, K., 1996, Postseismic rebound in fault step-overs caused by pore fluid: Science, v. 273, p. 1202–1204.

Picard, L., 1943, Structure and evolution of Palestine with comparative notes on neighboring countries: Jerusalem, Hebrew University Geological Department Bulletin 4, p. 1–187.

Poland, J.F., and Ireland, R.L., 1988, Land subsidence in the Santa Clara Valley, California, as of 1982: U.S Geological Survey Professional Paper 497-F, 61 p.

Rosen, P.A., Hensley, S., Zebker, H.A., Webb, F.H., and Fielding, E., 1996, Surface deformation and coherence measurements of Kilauea Volcano, Hawaii from SIR-C radar interferometry: Journal of Geophysical Research, v. 101, p. 23109–23125.

Sandwell, D.T., and Price, E.J., 1998, Phase gradient approach to stacking interferograms: Journal of Geophysical Research, v. 103, p. 30183–30204.

Scharroo, R., and Visser, P., 1998, Precise orbit determination and gravity field improvement for the ERS satellites: Journal of Geophysical Research, v. 103, p. 8113–8127.

Swarieh, A., Abu Al Adas, A., and Ghandoor, M., 2000, Sinkholes in Ghor Al Haditha area [abs.]: Maalot, Israel Geological Society Annual Meeting, p. 120.

Taqieddin, S.A., Abdelrahman, N.S., and Atallah, M., 2000, Sinkhole hazards along the eastern Dead Sea shoreline area, Jordan: A geological and geotechnical consideration: Environmental Geology, v. 39, p. 1237–1253.

Tarayre, H., and Massonnet, D., 1996, Atmospheric propagation heterogeneities revealed by ERS-1 interferometry: Geophysical Research Letters, v. 23, p. 989–992.

Terzaghi, K., 1925, Principles of soil mechanics, IV—Settlement and consolidation of clay: Engineering News-Record, v. 95, p. 874–878.

Tolman, C.F., and Poland, J.F., 1940, Ground-water, saltwater infiltration, and ground surface recession in Santa Clara Valley, Santa Clara County, California: Eos (Transactions, American Geophysical Union), v. 21, p. 23–24.

Wachs, D., Yechieli, Y., Shtivelman, V., Itamar, A., Baer, G., Goldman, M., Raz, E., Rybekov, M., and Schattner, U., 2000, Formation of sinkholes along the Dead Sea shore—Summary of findings from the first stage of research: Geological Survey of Israel Report GSI/41/2000, 49 p.

Werner, C.L., Hensley, S., Goldstein, R.M., Rosen, P.A., and

Zebker, H., 1992, Techniques and applications of SAR interferometry for ERS-1: Topographic mapping, change detection and slope measurement: Cannes, France, European Space Agency, First ERS-1 Symposium: Space at the service of our environment, p. 205–210.

Yechieli, Y., 1993, The effects of water level change in closed lakes (Dead Sea) on the surrounding groundwater and country rocks [Ph.D. thesis]: Rehovot, Israel, Weizmann Institute, 197 p. (in Hebrew with English abstract).

Yechieli, Y., Ronen, D., Berkowitz, B., Dershowitz, W.S., and Hadad, A., 1995, Aquifer characteristics derived from the interaction between water level of a terminal lake (Dead Sea) and an adjacent aquifer: Water Resources Research, v. 31, p. 893–902.

Zak, I., 1967, The geology of Mount Sedom [Ph.D. thesis]: Jerusalem, Hebrew University, 208 p.

Zebker, H.A., and Goldstein, R.M., 1986, Topographic mapping from interferometric synthetic aperture radar

observations: Journal of Geophysical Research, v. 91, p. 4993–4999.

Zebker, H.A., Werner, C.L., Rosen, P.A., and Hensley, S., 1994a, Accuracy of topographic maps derived from ERS-1 interferometric radar: IEEE Transactions on Geoscience and Remote Sensing, v. 32, p. 823–836.

Zebker, H.A., Rosen, P.A., and Goldstein, R.M., 1994b, On the derivation of coseismic displacement fields using differential radar interferometry: The Landers earthquake: Journal of Geophysical Research, v. 99, p. 19617–19634.

Zebker, H.A., Rosen, P.A., and Hensley, S., 1997, Atmospheric effects in interferometric synthetic aperture radar surface deformation and topographic maps: Journal of Geophysical Research, v. 102, p. 7547–7563.